

# Experimental Investigation of Zinc Antimonide Thin Film Thermoelectric Element over Wide Range of Operating Conditions

M. Mirhosseini<sup>1</sup>, A. Rezania<sup>1,\*</sup>, A. B. Blichfeld<sup>2,3</sup>, L. A. Rosendahl<sup>1</sup>

<sup>1</sup> Department of Energy Technology, Aalborg University, Pontoppidanstraede 111, 9220 Aalborg East, Denmark

<sup>2</sup> Centre for Materials Crystallography, Department of Chemistry and iNANO, Aarhus University, Langelandsgade 140, DK-8000 Aarhus C, Denmark

<sup>3</sup>Current address: Department of Materials and Engineering, Norwegian University of Science and Technology (NTNU), NO-7491, Trondheim, Norway.

## Abstract

Zinc antimonide compound is one of the most efficient thermoelectric (TE) materials known at moderate temperatures up to 350 °C for its exceptional low thermal conductivity. This study aims to evaluate performance of a thin film TE deposited on an insulating substrate, while the heat flows laterally in the thin film. At first, effect of applying different temperatures at hot side of the specimen is investigated to reach steady state in open circuit analysis. Then, the study focuses on performance and stability analysis of the thermoelectric element operating under different load resistances and over wide range of operating temperatures from 160 °C to 350 °C. The results show that, at hot side temperature equal to 275 °C, the Seebeck coefficient ( $\alpha$ ) reaches its maximum value (242  $\mu\text{V/K}$ ), which is comparable to that of bulk materials reported in the literature. According to variation of the load resistance, the maximum output power, that is a function of temperature, occurs at 170.25  $\Omega$ . The maximum power is 8.46  $\mu\text{W}$  corresponding to a cold and hot side temperature of  $\approx 30$  °C and 350 °C, respectively.

**Keywords:** *Thin Film TEG; Maximum Output Power; Seebeck Coefficient; Zinc Antimonide; Load Resistance.*

## 1. Introduction

Thermoelectric (TE) devices have been employed for many years as a reliable energy conversion technology for applications ranging from the cooling devices to the direct conversion of heat into electricity for power generation.

---

\* Corresponding author: Alireza Rezaniakolaei. E-mail: [alr@et.aau.dk](mailto:alr@et.aau.dk)

26 The efficiency of TE materials is evaluated using the dimensionless figure of merit,  $zT = \alpha^2 T / (\rho \kappa)$ , where  $\alpha$  is the  
27 Seebeck coefficient,  $T$  is absolute temperature,  $\rho$  is electrical resistivity and  $\kappa$  is the total thermal conductivity consisting  
28 of contribution from the charge carrier  $\kappa_e$  and the lattice  $\kappa_L$ . TE materials with  $zT > 1$  can typically give a reasonable  
29 efficiency (e.g. 5%), but in fact for commercial applications it is equally important that the TE materials are made of  
30 cheap and abundant elements with cost-effective synthesis methods [1].

31 Although most research concerns bulk materials for high power applications such as recovery of waste heat from car  
32 exhaust, attractive low power applications of thin films are evident. The inherent phonon scattering due to the  
33 nanostructure of thin films can be exploited to enhance TE properties [2]. As a new kind of environmentally friendly  
34 material, ZnSb is made of relatively cheap and nontoxic elements.

35 The Zn–Sb binary system contains ZnSb and  $\beta$ -Zn<sub>4</sub>Sb<sub>3</sub> which are promising p-type thermoelectric materials for low cost  
36 thermoelectric application, intended to operate at intermediate temperatures (from room temperature to 350 °C) [3].

37 Thin film technique is a promising method for improving the thermoelectric properties of thermoelectric material due to  
38 low dimensional quantum confinement and a much lower lattice thermal conductivity [4]. Properties of the thin film  
39 thermoelectric materials have introduced a huge potential in application of miniaturization sensors, micro-power source  
40 and other thermoelectric applications of the thin film thermoelectric devices. Moreover, for many micro scale TE  
41 devices, thin films are highly required [5]. Therefore, thin films can offer tremendous scope for enhancement the figure  
42 of merit. There are some researches for basic evaluation of TEG devices or samples under different conditions, where  
43 very few of them are based on zinc antimonide TE material. The efficiency of a commercial TEG under thermal cycling  
44 was investigated by Hatzikraniotis *et al.* [6]. They investigated long time performance and stability of a commercially  
45 available TEG under variable temperature and load cycling. The module was subjected to sequential hot side heating (at  
46 200 °C) and cooling for long times (3000 h) in order to measure changes in the TEG's performance. A reduction of  
47 3.8% in Seebeck coefficient, a 16.1% increase in resistivity and 6.6% decrease in the average leg thermal conductivity  
48 were observed. In a study by Sun *et al.* [7], zinc antimonide films were deposited on polished fused silica substrates by  
49 co-sputtering of a Zn target and a specifically prepared Zn-Sb compound target. The TE measurements were subjected  
50 to two measurement cycles, *i.e.* room temperature ( $RT$ )  $\rightarrow$  573 K  $\rightarrow$   $RT$   $\rightarrow$  573 K  $\rightarrow$   $RT$ . It was seen that the TE  
51 properties of the film become stable after the first heating cycle. The stable power factor (PF) of their Zn<sub>4</sub>Sb<sub>3</sub> film  
52 during the two measurement cycles implied a good phase stability of Zn<sub>4</sub>Sb<sub>3</sub> at  $T \leq 573$  K in a low pressure inert  
53 atmosphere.

54 Yan and Malen [8] showed that the use of a periodic heat source, instead of a constant heat source, can improve the  
55 conversion efficiency of a thermoelectric power generator. In addition, they presented experimental measurements on a  
56 commercial thermoelectric device (bismuth telluride based device) to validate analytical and numerical models. These  
57 models showed that maximum efficiency is achieved when the period of the heat source is much larger than the thermal  
58 time constant of the thermoelectric power generator.

59 In a study on zinc antimonide compounds [3], it was found that the thermoelectric properties of Zn-Sb thin films are  
60 sensitively related to the phase transformation. The deposited thin films were annealed at 673 K under Ar atmosphere  
61 for 1 hr. X-ray diffraction (XRD) results showed that the thin film gradually transforms from  $\beta$  phase  $Zn_4Sb_3$  to ZnSb  
62 phase with increasing Sb sputtering power. Moreover, an enhanced power factor of  $1.91 \times 10^{-3} \text{ W/m K}^2$  was obtained  
63 through optimizing the ratio of  $\beta$ - $Zn_4Sb_3$  to Zn-Sb phase in the mixed Zn-Sb thin film. For all the specimens, Seebeck  
64 coefficient increased by temperature from 300 to 573 K.

65 Zinc antimonide thin film specimens were deposited on polyimide substrate by radio frequency sputtering method at  
66 room temperature [9]. All the specimens were annealed in argon atmosphere at different temperatures and the  
67 thermoelectric properties of all the thermoelectric elements were significantly boosted. The power factor of thin films  
68 annealed at 325 °C was higher than other specimens. After improving properties, the specimens were tested in different  
69 working temperatures from 50 to 260 °C. The maximum Seebeck coefficient of  $280 \mu\text{V K}^{-1}$  and the maximum power  
70 factor of  $2.35 \times 10^{-3} \text{ Wm}^{-1} \text{ K}^{-2}$  was obtained at 260 °C.

71 Fan *et al.* [10] demonstrated a promising flexible thin film thermoelectric generator using the n-type Al-doped ZnO and  
72 p-type Zn-Sb based thin film. Their flexible substrate was suitable to be used under 520 K. They showed that the output  
73 power of their generator is 4 times higher than those in the literature, while it is 4-5 times cheaper.

74 Brinks *et al.* [11] investigated on thermal stability enhancement of thermoelectric  $Ca_3Co_4O_9$  thin films up to 550 °C in  
75 an oxygen rich environment. The thermal stability and high temperature thermoelectric properties were studied by  
76 electrical resistivity and Seebeck measurements by thermal cycling. In contrast to generally performed heating in  
77 helium gas, it was shown that an oxygen/helium mixture provides sufficient thermal contact, while preventing the  
78 previously disregarded formation of oxygen vacancies. The resistivity is much more sensitive to the background gas  
79 during thermal cycling than the Seebeck coefficient in thin film and bulk  $Ca_3Co_4O_9$ .

80 In another study on thin film TEGs, Daniel *et al.* [12] studied thermal stability of thermoelectric  $CoSb_3$  skutterudite thin  
81 films. It was shown that an excess of Sb stabilizes the  $CoSb_3$  skutterudite phase. Furthermore, resistivity was stable  
82 during thermal cycling as long as the temperature was kept below the initial annealing temperature.

83 Shim *et al.* [13] discovered that, as the number of thermal cycle increases, the power factor of  $Zn_xSb_y$  thin films is  
84 reduced. This degradation is more pronounced in an inert gas atmosphere than in ambient surroundings. The main  
85 reason of this degradation was closely related to the reduction in the electrical conductivity of the  $Zn_xSb_y$  thin film,  
86 which is associated with thermal decomposition. Fan *et al.* [14] demonstrated the properties of their designed thin film  
87 thermoelectric generators with heat flow running in longitudinal direction of the film, where the maximum temperature  
88 difference between both sides is maintained 85 °C. N-type  $Bi_2Te_3$  and p-type  $Sb_2Te_3$  thin films were deposited on soda-  
89 lime glass substrates. They argued that the performance of thin film TEG with this structure can be further improved by  
90 optimizing thermoelectric materials and fabrication methods. In a conventional thin film TEG as reported in most of the  
91 above references, heat flow running perpendicular to the film surface is widely used. In these thin films, the hot side and  
92 cold side are just separated by the thickness of the films. The temperature of the cold side increases immediately by the  
93 heat transferred from the hot side, and the temperature difference between both sides will be alleviated greatly in a very  
94 short time. Due to the small temperature difference, conventional thin films usually have low output power even though  
95 the figure of merit of the materials used for thin films is high. This kind of TE modules needs an efficient cooling  
96 technology with high cooling energy to keep the cold side temperature low that is not efficient from aspect of net  
97 energy and economy. Accordingly, to produce more electrical potential difference by using thin film based  
98 thermoelectric module, one way is that heat flow runs lateral to the surface of thin films deposited on an insulating  
99 substrate. One advantage of using the thermoelectric element laterally is that, due to high thermal resistance of the  
100 thermoelectric element, there is no need for an efficient heat sink in order to provide an efficient TE module.  
101 There are only references [10, 14] which discuss only about the thermoelectric properties of a thin film p-n couple and  
102 modules in steady state which heat conducts in the longitudinal direction parallel to thin film surface by using constant  
103 hot side temperatures when the cold side is exposed to the environmental temperature. Therefore, present study  
104 investigates the performance of a zinc antimonide specimen as a p-type leg of a TE module under transient as well as  
105 steady state thermal boundary condition close to practical conditions.

106

## 107 **2. Experimental apparatus and procedures**

### 108 **2.1. Thin film production**

109 The thin films are produced by magnetron co-sputtering deposition at Aarhus University, Denmark. The Zn-Sb film was  
110 directly deposited on fused silica substrates. One target was a commercial Zn-target, whereas the other was produced in-

111 house by the process reported by Yin *et al.* [15]. The substrate is a 180  $\mu\text{m}$  thick single-sided polished fused silica  
112 wafer. The substrate was heated to 215  $^{\circ}\text{C}$  during the deposition, to allow for crystallization of the film. Argon (purity  
113 99.9996%) was used as sputter gas at a flow rate of 10 sccm and the Ar pressure in the chamber was fixed at 0.6 Pa with  
114 a deposition time of 60 minutes. The power for the  $\text{Zn}_4\text{Sb}_3$  and Zn targets were fixed to 12 W and 4 W, respectively.  
115 The chamber base pressure was approximately  $3 \times 10^{-5}$  Pa. The phase transitions of the film were confirmed directly by  
116 in situ powder X-ray diffraction (PXRD) and further evidenced through the changes in the electrical properties. The as-  
117 deposited and annealed specimen was characterized by SEM (Nova600 NanoLab, FEI) with EDX, PXRD (D8  
118 Discover, Bruker AXS) in  $\theta - 2\theta$  geometry with  $\text{CuK}\alpha$  radiation, and in situ PXRD. The film thickness is about 600 nm,  
119 which was measured from the cross sectional SEM image. Before and after the annealing treatment, no change of the  
120 film thickness was observed.

121 This thermoelectric element has been produced with atomic ratio (Zn:Sb) as mentioned in Table 1. This is roughly the  
122 same as for the Zn-Sb film reported by Sun *et al.* [7]. XRD pattern is shown in Fig. 1 for the specimen.

123 The ratio of ZnSb:  $\text{Zn}_4\text{Sb}_3$  is  $\sim 6:4$ , so ZnSb is the dominant phase. The photograph of this specimen before the tests is  
124 also shown in Fig. 1. The specimen is a rectangular thin film by the length and width equal to 19.8 and 17.2 mm,  
125 respectively. The length of hot side and cold side contact area is equal to 3 mm that should be subtracted from the total  
126 length to obtaining the effective length.

127

## 128 **2.2. Thin film test bench**

129

130 The test device integrated on the bench (Fig. 2) with ability of heating the hot side up to 400  $^{\circ}\text{C}$ . This device is for  
131 testing any kind of coated TE thin film thermoelectric elements and TE single legs. There is integrated separately  
132 cooling system of the cold side, but in the present study by assuming environmental temperature for the cold side of the  
133 specimen, this part of the test bench is not used. Thus, the cold side of the specimen is only in contact with cold side  
134 block without any forced convection cooling during the test. The temperature of the hot side can be adjusted between  
135 150  $^{\circ}\text{C}$  and 400  $^{\circ}\text{C}$ . The hot and cold side temperatures are measured by probes mounted on both sides of the specimen.  
136 In the present study, a wide range of temperatures at the hot side and room temperature at the cold side of the specimen  
137 are applied in order to measure performance of the thin film element. Nine temperatures at hot side of the specimen are  
138 provided; 160, 175, 200, 225, 250, 275, 300, 325, and 350  $^{\circ}\text{C}$ . After some minutes from the beginning of each test, the

139 specimen operates under steady state condition. Whole measurement time by data logger is 4500 seconds for each  
140 experiment. Data sampling rate was 0.25 Hz, giving 300 data points for each test.

141

### 142 **3. Results and discussion**

#### 143 **3.1. Open circuit analysis**

144

145 Fig. 3 shows the hot side temperature of the specimen during the time. According to the figure, the condition can be  
146 assumed steady state after a short transient region. In Fig.4, voltages versus time are observed. Voltage in open circuit  
147 condition has similar trend with the hot side temperature with respect to time.

148 Variation of the voltage versus temperature difference ( $\Delta T = T_{\text{hot}} - T_{\text{cold}}$ ) is shown for different hot side temperatures in  
149 Fig.5. The trend of the figure is approximately linear for all cases, showing that the voltage is increasing by raising the  
150 temperature difference for all cases almost with the same slope. According to different hot side conditions, passing from  
151 unsteady area is not exactly the same even in the same temperature difference. It is due to several parameters such as  
152 thermal diffusivity which can change by temperature. In other words, in the transient area, there is not exactly a single  
153 voltage data point for each temperature difference since different boundary conditions are applied. In each data set, the  
154 voltage data points in transient condition are dispersed, while the data points related to the steady state condition are  
155 obviously aggregated. When the system is thermally balanced and reached the steady state condition, almost 280 data  
156 points are collected which are much closer together unlike the transient conditions.

157 Moreover, in sub-Fig.5, the voltage versus hot side temperatures is shown for steady state condition. The figure has  
158 been obtained by end values of voltage at colored marker data sets in Fig. 5. It seems a linear approximation will also be  
159 a convenient fitting for the sub-Fig. 5.

160 The Seebeck coefficient ( $\alpha$ ) versus the hot side temperature is shown in Fig.6. Using the hot and cold side temperatures  
161 and the voltage to calculate instantaneous Seebeck coefficient shows interesting trend of this coefficient until the steady  
162 state condition is reached. Nevertheless, definition of the Seebeck coefficient could be applicable also in transient  
163 conditions; under such conditions where it can be named as transient Seebeck coefficient.

164 When the accumulation of the data points related to the maximum hot side temperature increases to its extreme, it  
165 means the system reaches steady state condition; where the final value of these Seebeck coefficients occurs.

166 The obtained value of  $\alpha$  for this specimen is in agreement with new developed TEG materials and zinc antimonide  
167 compounds in literature [7, 9-11, 13, 16].

168 The values of Seebeck coefficient with respect to time are shown in Fig. 7. It is worthy to mention that the Seebeck  
169 coefficient is a material's property. The first data point in each data set is related to data recorded at the moment the  
170 heater is turned on. In other words, the first calculated value of Seebeck coefficient is equal to the Seebeck coefficient  
171 in ambient temperature. Ignoring the first data point, the rate of increasing the temperature difference between the  
172 specimen's junctions is lower than increasing the voltage in a short range of transient area. That is due to higher thermal  
173 conductivity of ZnSb at lower temperature ranges, whereas it decreases by increasing the temperature [7, 13]. In  
174 continue, in the rest of the transient area, the rate of increasing the temperature difference is higher than increasing the  
175 voltage and the value of transient Seebeck coefficient is alleviated to reach its own steady state values. In steady area,  
176 these values are very close to each other during the tests in spite of different thermal conditions.

177 With a detailed evaluation of the Seebeck coefficients in steady state in Fig.8, this coefficient varies with different  
178 thermal conditions. This figure is a criterion for clear comparison of Seebeck coefficients versus the hot side or average  
179 temperature of the specimen. The Seebeck coefficient is observed to increase up to a maximum (242  $\mu\text{V/K}$ ) and then  
180 decreases. Although, its variation is negligible especially for operating temperature of hot side between 275 °C and 350  
181 °C, but the maximum point is interesting. Herein, the contribution of the third factor of thermal conductivity to the total  
182 thermal conductivity is appeared, namely bipolar transport. When the hot side temperature increases more than 275 °C,  
183 the bipolar transport effect arises because of the two types of charge carriers, namely electrons and holes. The bipolar  
184 transport increases due to the excitation of electrons from the valence band to the conduction band as the temperature is  
185 increased, creating an equal number of holes. These holes and electrons will then move to the cold side and transport  
186 heat from the hot side to the cold side of the specimen. However, the net electrical current is zero in this movement due  
187 to the equal numbers of opposite charges, but finally, the presence of both electrons and holes will have a negative  
188 effect on the Seebeck coefficient. Therefore, bipolar effect happens whenever the temperature of the whole  
189 thermoelectric element or even a part (section) of it is more than an individual temperature which related to the type of  
190 material, its manufacturing process and impurities in its structure, etc. In other words, bipolar affects the whole body of  
191 the TE specimen or device and its characteristics such as total Seebeck coefficient, electrical resistivity, and thermal  
192 conductivity, even if it happens only near the hot side.

193 The trend of Seebeck coefficient by increasing the temperature is similar to the results in reference [16] for zinc  
194 antimonide specimen without doping by silver (Ag). In sub-Fig. 8, Seebeck coefficient is shown for a thin film that has

195 been previously produced by the same procedure and composition [7]. It can be observed that the bipolar transport  
 196 happens near the temperature 263 °C, whereas in our study, it happens in hot side temperature 275 °C. Thus, bipolar  
 197 transport happens almost in the same temperature. Certainly, this device and procedure for testing the thin film  
 198 specimen is different with the device and method that they used in their study [7]. Figure 9 shows the electrical  
 199 resistivity of the specimen versus time. In Fig. 10, the electrical resistivity and thermal conductivity of the  
 200 thermoelectric element are represented for various average temperatures in steady state condition. Both data series in  
 201 the figure reduce slightly by raising the hot site temperature. By using the relation 1 and 2 for calculating the figure of  
 202 merit ( $ZT$ ) and efficiency ( $\eta$ ), Fig. 11 is drawn. In these calculations, the Seebeck coefficient that was shown in Fig. 8,  
 203 and thermal conductivity and electrical resistivity from Fig. 10 are used.

$$204 \quad ZT = \frac{\alpha^2 T}{\rho \kappa} \quad (1)$$

$$205 \quad \eta = \frac{T_h - T_c}{T_h} \frac{\sqrt{1 + ZT} - 1}{\sqrt{1 + ZT} + \frac{T_c}{T_h}} \quad (2)$$

206 where  $\alpha$  is the Seebeck coefficient [V/K],  $T$  [K] is the mean temperature of the thermoelectric element,  $\rho$  [ $\Omega \cdot m$ ] is the  
 207 electrical resistivity,  $\kappa$  [W/m.k] is the thermal conductivity,  $T_h$  and  $T_c$  are hot and cold side temperature, respectively.

208 As seen in Fig. 11, by increasing the hot side temperature, both figure of merit and efficiency increase. The maximum  
 209 efficiency of the specimen in this operating condition is about 7.4%. The hump on the figure of merit curve (at hot side  
 210 temperature 275 °C) is directly related to Seebeck coefficient values trend (Fig. 8) as seen in equation 1. But, the hump is  
 211 not clearly disclosed in the curve of efficiency. The results in Figs. 10 and 11 are brought versus average temperature to  
 212 be comparable with the results of reference [7] in the mentioned temperature range.

213

### 214 **3.2. Close circuit analysis**

215 In this part, the study focuses on stability analyzing of power generation by the specimen operating under different load  
 216 resistances at above mentioned thermal conditions in steady state.

217 A wide range of load resistance (from 10 to 300  $\Omega$ ) is applied with a 10  $\Omega$  step to find optimal electrical load value  
 218 giving the maximum power generated by the specimen. It must be mentioned that at first the specimen thermally  
 219 reaches steady state condition without load, and then the load is applied. Whenever the under loaded thermoelectric  
 220 element reaches steady state condition, as electronically at each temperature, the next higher load is applied. The time



221 interval for each load value is chosen 5 minutes to ensure the thermoelectric element reaches steady state condition  
222 under the applied electrical load.

223 Based on theory, maximum power is produced when the value of the external load is equal to the thermoelectric  
224 element resistance. In the present study, due to unavoidable contact resistance, the maximum output power happens  
225 when the external load is equal to the thermoelectric element resistance plus contact resistance. Internal resistance of the  
226 thermoelectric element plus contact resistance in environment temperature is equal to 188.3  $\Omega$ . By having the electrical  
227 resistivity (from Fig. 10) and the geometry of the thermoelectric element, internal resistance of it can be calculated by  
228 relation 3.

229

$$230 \quad R = \frac{\rho L}{A} \quad (3)$$

231 where  $L$  and  $A$  are the effective length and cross section area of the specimen, respectively.

232 Due to restriction for bracing the thermoelectric element (comprised thin glass substrate) in joint locations, the amount  
233 of contact resistance in a real application inevitably is several times more than the internal resistance of the specimen.  
234 The thermoelectric element electrical resistance will have a huge difference to that one including contact resistance  
235 shown in Fig. 12; but the value of both of them is slightly decreasing by raising the temperature. Testing the specimen  
236 by different loads shows that peak power is produced in a load resistance very close to the slope of V-I linear  
237 distribution, separately for each thermal condition. Also, for all curves in Fig. 13, power increases to a maximum value,  
238 and decreases afterwards. The maximum power occurs at external loads 170-190  $\Omega$ . The peak power is 8.46  $\mu\text{W}$   
239 corresponding to the hot side temperature 350  $^{\circ}\text{C}$  and external load equal to 170.25  $\Omega$ ; whereas the peak power by the  
240 specimen without considering contact resistance effect can be calculated by relation 4 and is 127.21  $\mu\text{W}$  (Fig. 14).

$$241 \quad P = \frac{\alpha^2 (\Delta T)^2 A}{\rho L} \quad (4)$$

242

243 The percentage of difference between two series of results in Fig. 14 is about 93-94%, that shows the improvement of  
244 electrical conductivity at contact locations can reduce the waste power seriously. At the end of tests, further open  
245 circuit tests are taken to check degradation of the Seebeck coefficient to ensure stability of the thermoelectric element  
246 during the tests.

247

#### 248 **4. Conclusions**

249 An efficient thin film TEG module based on p-n couples can be designed and fabricated since a fundamental  
250 investigation is firstly done to analyze the performance of the uni-thin film specimen. Present study investigated  
251 performance of a zinc antimonide thermoelectric element as a p-type leg of a TE module in transient and steady state  
252 under different operating conditions representing practical conditions. To produce more electrical power by using thin  
253 film specimen, the heat flow runs laterally in the thermoelectric element. The Transient Seebeck coefficient is  
254 introduced in details to analyze behavior of the thermoelectric element. The results show that the Seebeck coefficient in  
255 steady state condition increased to a maximum value (242  $\mu\text{V/K}$ ) and then reduces as the hot side temperature increases.  
256 The bipolar transport is the main reason of reducing the Seebeck coefficients from hot side temperature 275  $^{\circ}\text{C}$  to 350  
257  $^{\circ}\text{C}$ . It is shown that the bipolar transport effect is a localized phenomenon. This study considered stability behavior  
258 tracking of the thermoelectric element operating under different load conditions at wide range of temperature. The  
259 obtained load resistance corresponding to peak power output is shown to be a function of temperature. Also, by  
260 increasing the hot side temperature, the maximum output power, figure of merit, and the efficiency of the specimen is  
261 enhanced. The thin film specimen showed that can operate in relatively high range of temperature with long operation  
262 period without failure or degradation in its thermoelectrically performance.

263

## 264 **Acknowledgment**

265 This work was carried out within the framework of the Center for Thermoelectric Energy Conversion (CTEC) and is  
266 funded in part by the Danish Council for Strategic Research, Programme Commission on Energy and Environment,  
267 under Grant No. 63607.

268

## 269 **References**

- 270 [1] G.J. Snyder, E.S. Toberer, *Nat. Mater.* 105, 7 (2008).
- 271 [2] C.J. Vineis, A. Shakouri, A. Majumdar, M.G. Kanatzidis, *Adv. Mater.* 3970, 22 (2010).
- 272 [3] Z.H. Zheng, P. Fan, P.J. Liu, J.T. Luo, X.M. Cai, G.X. Liang, D.P. Zhang, F. Ye, Y.Z. Li, Q.Y. Lin, *Appl. Surf. Sci.*  
273 823, 292 (2014).
- 274 [4] H. Ohta, S.W. Kim, Y. Mune, T. Mizoguchi, K. Nomura, S. Ohta, T. Nomura, Y. Nakanishi, Y. Ikuhara, M. Hirano,  
275 H. Hosono, K. Koumoto, *Nat. Mater.* 129, 6 (2007)

- 276 [5] Z.H. Zheng, P. Fan, J.T. Luo, P.J. Liu, X.M. Cai, G.X. Liang, D.P. Zhang, Y. Fan, *Intermetallics*. 18, 64 (2015).
- 277 [6] E. Hatzikraniotis, K.T. Zorbas, I. Samaras, T.H. Kyratsi, K.M. Paraskevopoulos, *J. Electron. Mater.* 2112, 39
- 278 (2010).
- 279 [7] Y. Sun, M. Christensen, S. Johnsen, N.V. Nong, Y. Ma, M. Sillassen, E. Zhang, A.E.C. Palmqvist, J. Bøttiger, B.B.
- 280 Iversen, *Adv. Mater.* 1693, 24 (2012).
- 281 [8] Y. Yan, J.A. Malen, *Energy Environ. Sci.* 1267, 6 (2013).
- 282 [9] P. Fan, W.F. Fan, Z.H. Zheng, Y. Zhang, J.T. Luo, G.X. Liang, D.P. Zhang, *J. Mater. Sci: Mater. Electron.* 5060, 25
- 283 (2014).
- 284 [10] P. Fan, Z.H. Zheng, Y.Z. Li, Q.Y. Lin, J.T. Luo, G.X. Liang, X.M. Cai, D. Zhang, F. Ye, *Appl. Phys. Lett.* 106
- 285 (2015).
- 286 [11] P. Brinks, N.V. Nong, N. Pryds, G. Rijnders, M. Huijben, *Appl. Phys. Lett.* 143903, 106 (2015).
- 287 [12] M.V. Daniel, M. Friedemann, J. Franke, M. Albrecht, *Thin Solid Films.* 203, 589 (2015).
- 288 [13] H.C. Shim, C.S. Woo, S. Han, *ACS Appl. Mater. Interfaces.* 17866, 7 (2015).
- 289 [14] P. Fan, Z.H. Zheng, Z.K. Cai, T.B. Chen, P.J. Liu, X.M. Cai, D.P. Zhang, G.X. Liang, J.T. Luo, *Appl. Phys. Lett.*
- 290 033904, 102 (2013).
- 291 [15] H. Yin, A.B. Blichfeld, M. Christensen, B.B. Iversen, *ACS Appl. Mater. Interfaces.* 10542, 6 (2014)
- 292 [16] D.B. Xiong, N.L. Okamoto, H. Inui, *Scripta Materialia.* 397, 69 (2013).

293  
294  
295  
296  
297  
298  
299  
300  
301  
302  
303  
304

305  
306  
307  
308  
309  
310  
311  
312  
313  
314  
315  
316  
317  
318  
319  
320  
321  
322  
323  
324  
325  
326  
327  
328  
329  
330

**Figures**

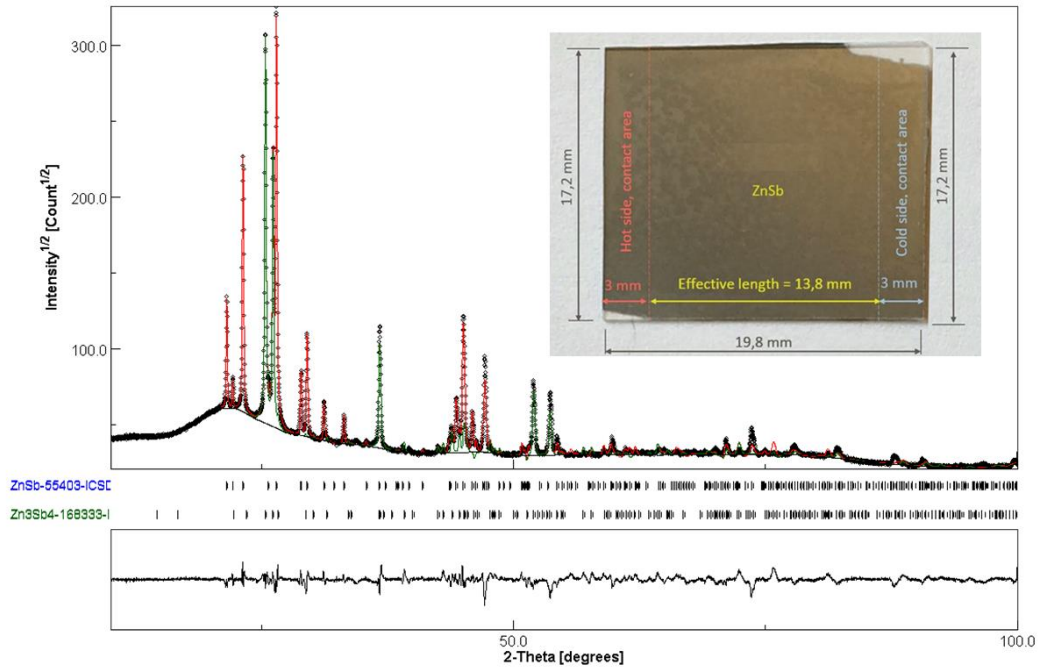
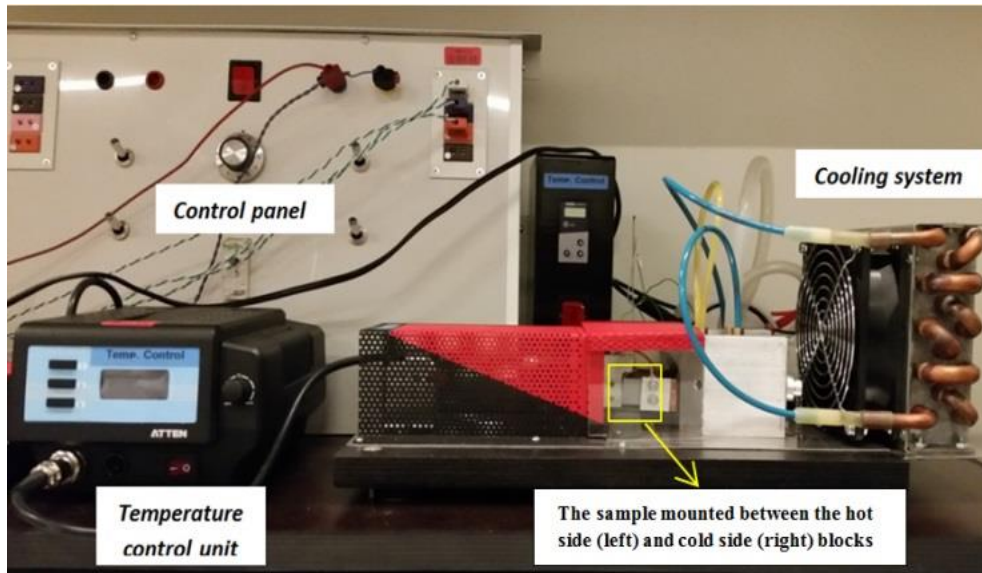
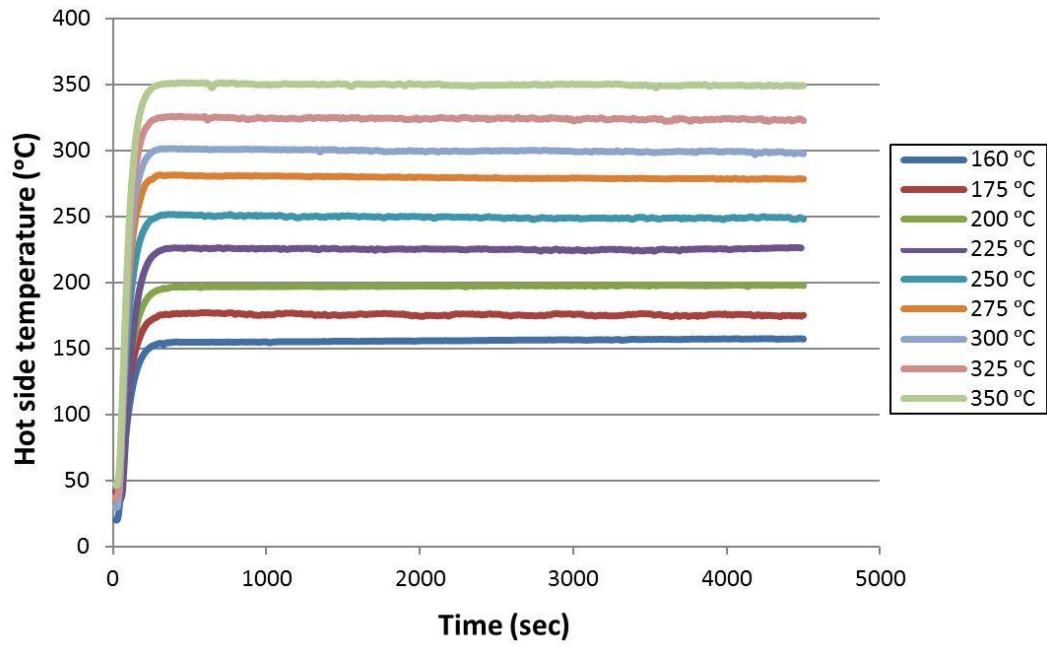


**Fig.1: XRD patterns of Zn-Sb thin film and geometric parameters of the specimen**



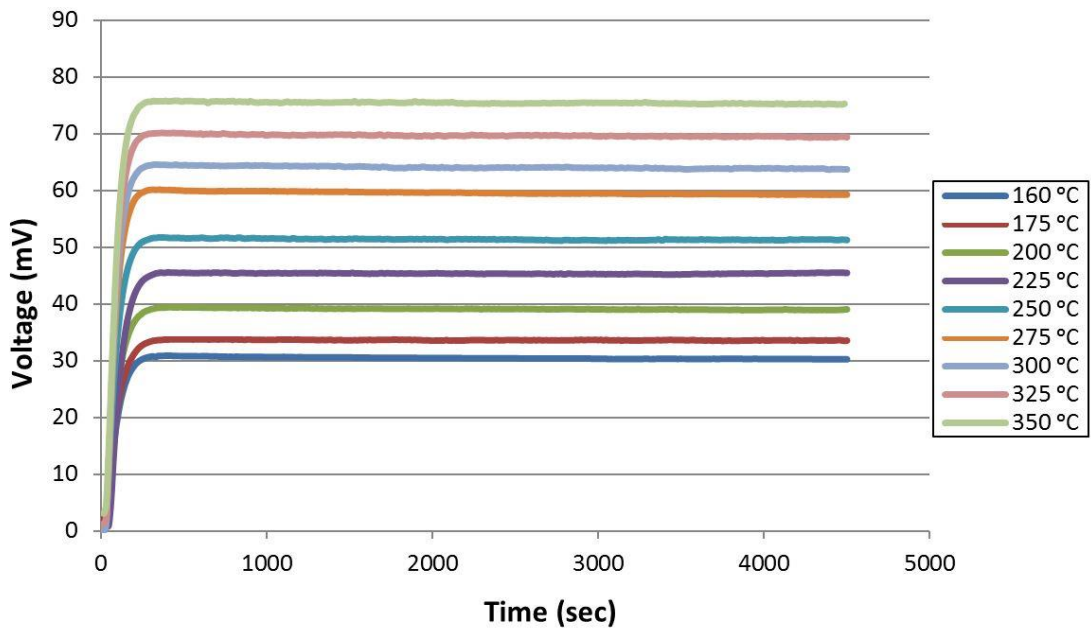
331  
332  
333  
334  
335  
336

**Fig.2: Experimental apparatus**



337  
338  
339

**Fig.3: Hot side temperature versus time**

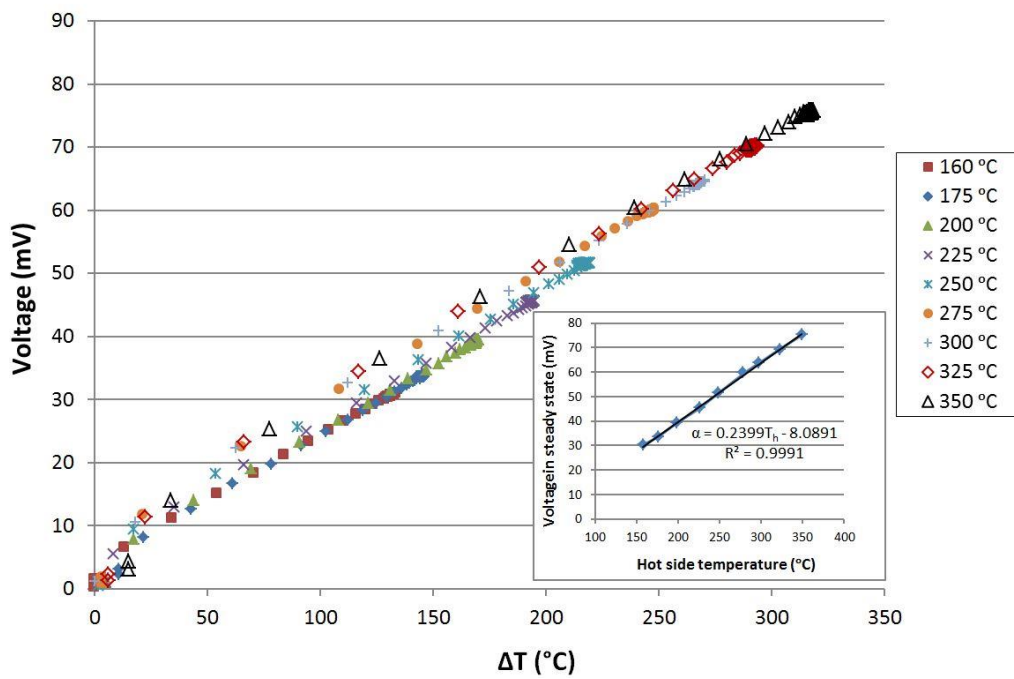


340

341

Fig.4: Voltage at different hot side temperatures versus time

342



343

344

Fig.5: Voltage versus temperature difference, and voltage in steady state versus different hot side temperatures

345

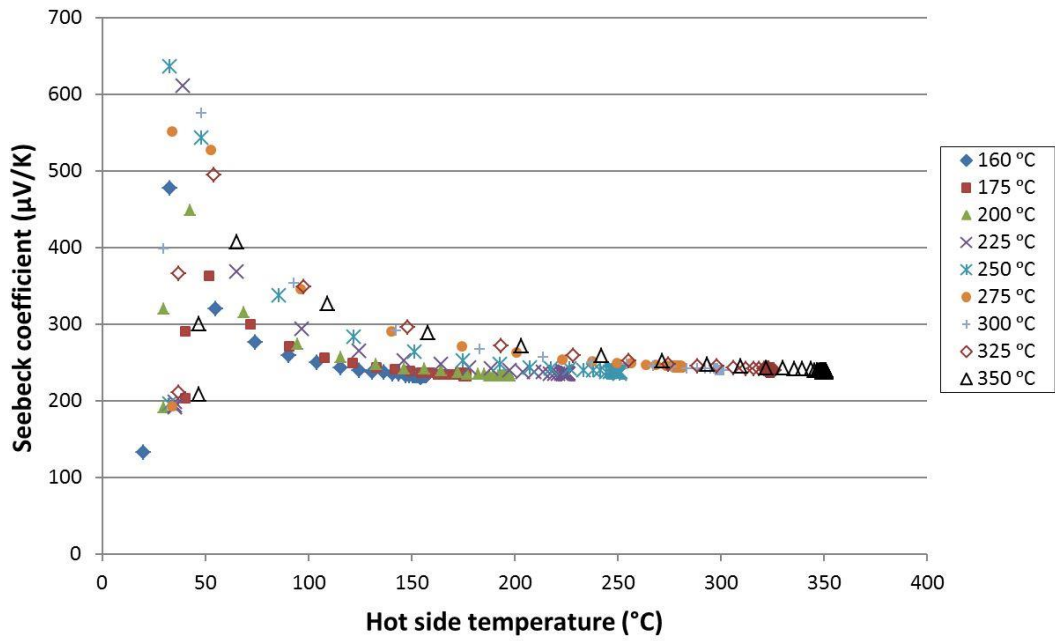


Fig.6: Seebeck coefficient versus hot side temperature

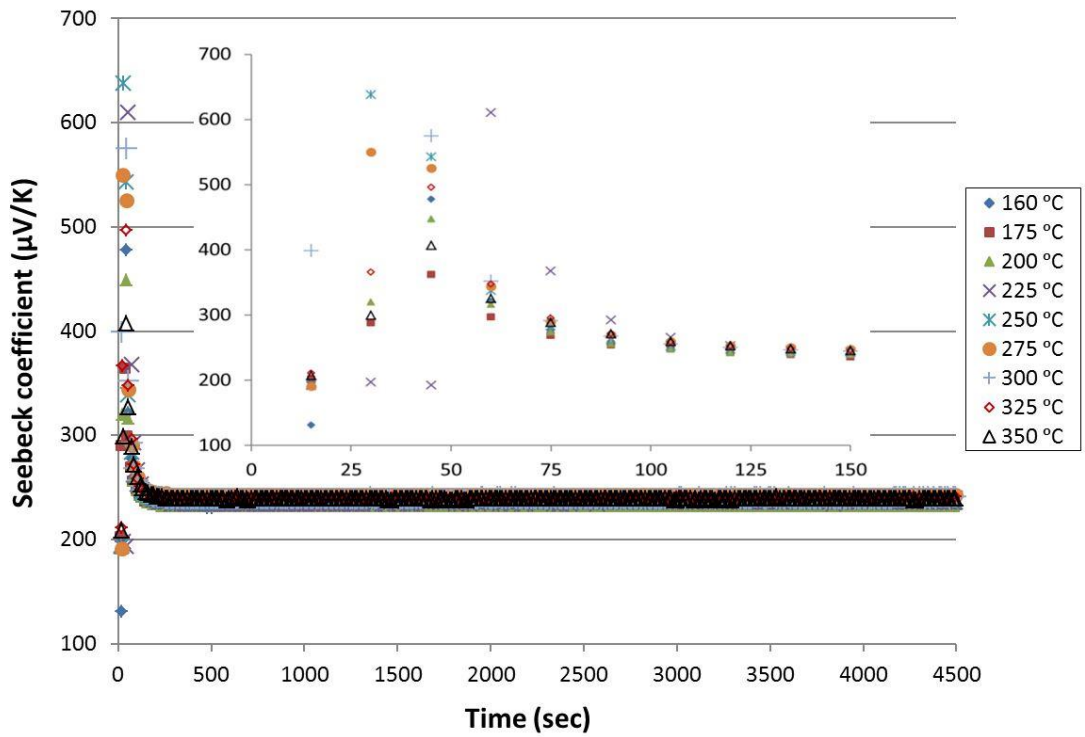


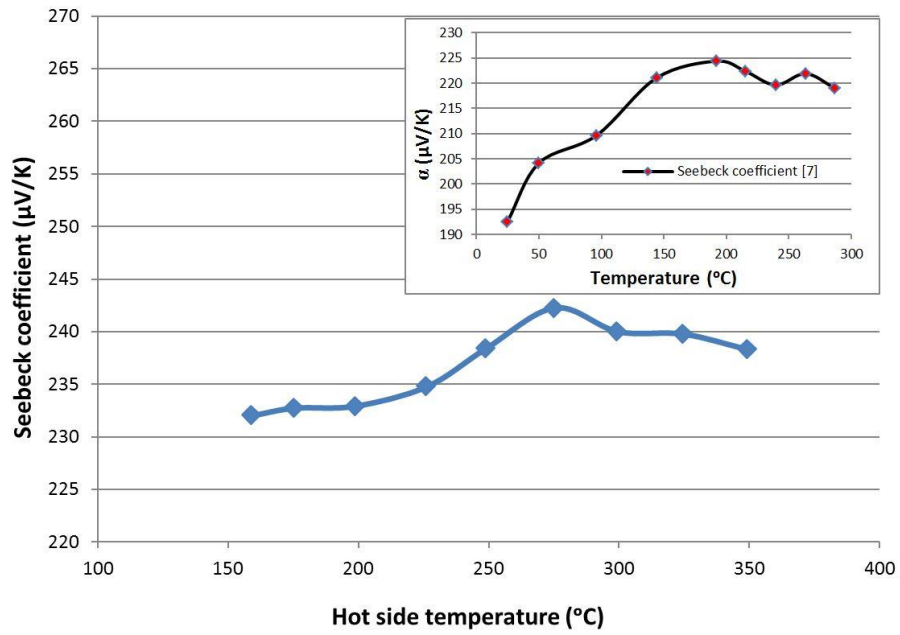
Fig.7: Seebeck coefficient versus time

346  
347  
348  
349

350  
351

352

353



354

355

Fig.8: Seebeck coefficient in steady state versus hot side temperature of the specimen

356

357

358

359

360

361

362

363

364

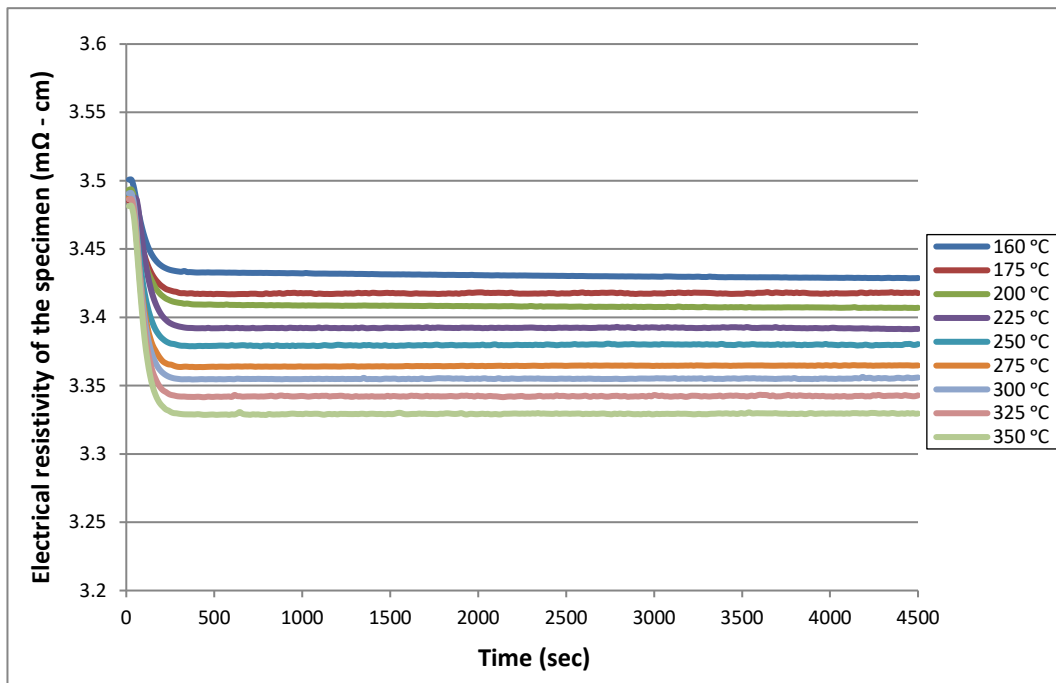
365

366

367

368

369





370  
371  
372  
373  
374  
375  
376  
377  
378  
379  
380  
381  
382  
383  
384  
385  
386  
387  
388  
389  
390  
391  
392  
393  
394  
395  
396  
397

**Fig.9: Electrical resistivity of the specimen versus time**

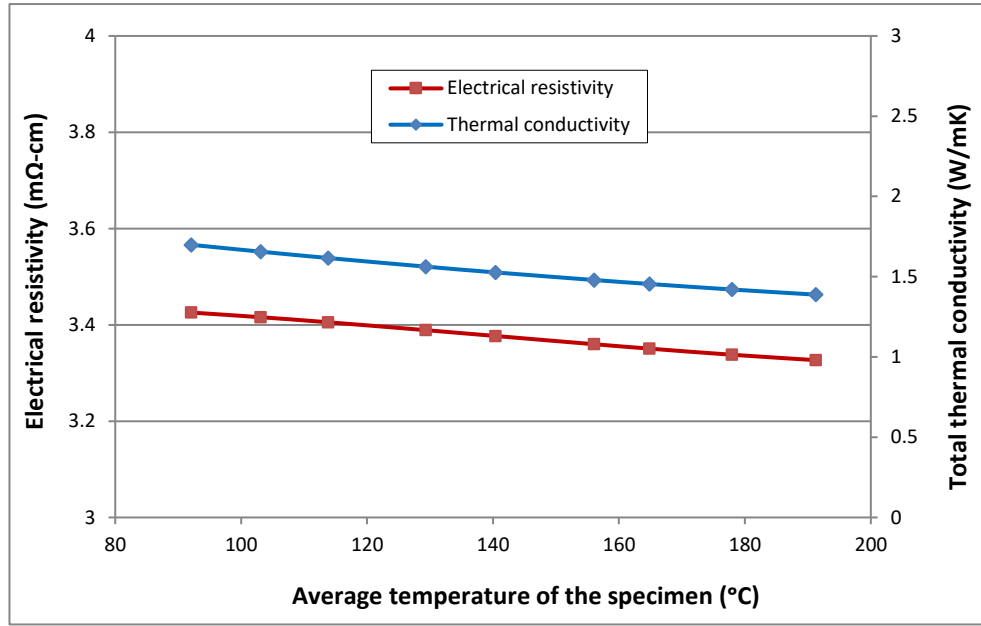


**Fig. 10: Electrical resistivity and thermal conductivity in steady state versus average temperature of the specimen**

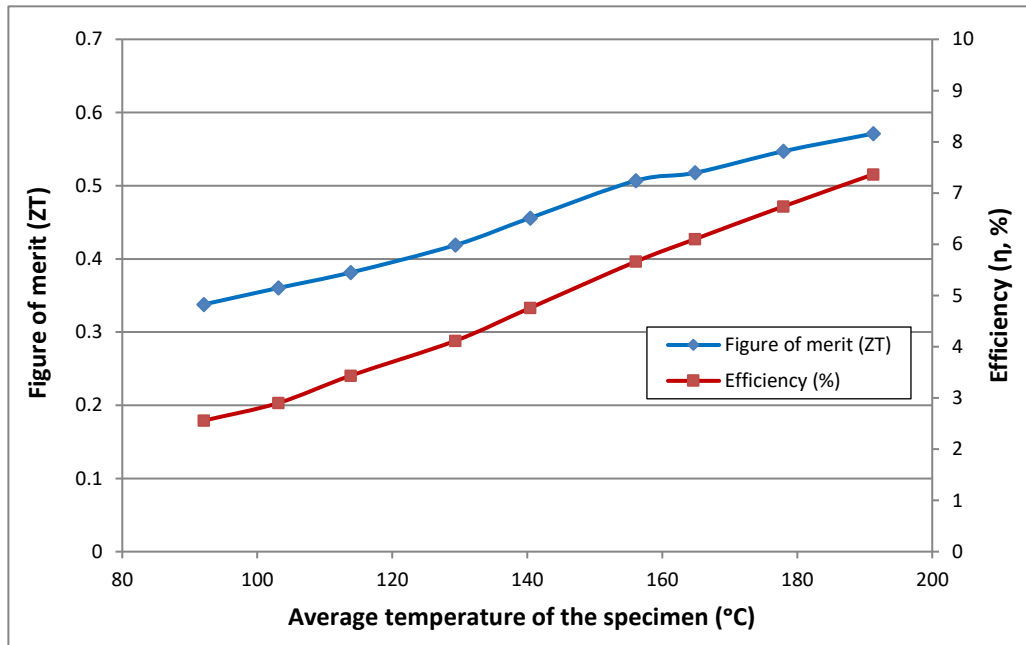


**Fig. 11: Figure of merit and efficiency of the thermoelectric element versus average temperature**

398  
 399  
 400  
 401  
 402  
 403  
 404  
 405  
 406  
 407  
 408  
 409  
 410  
 411  
 412

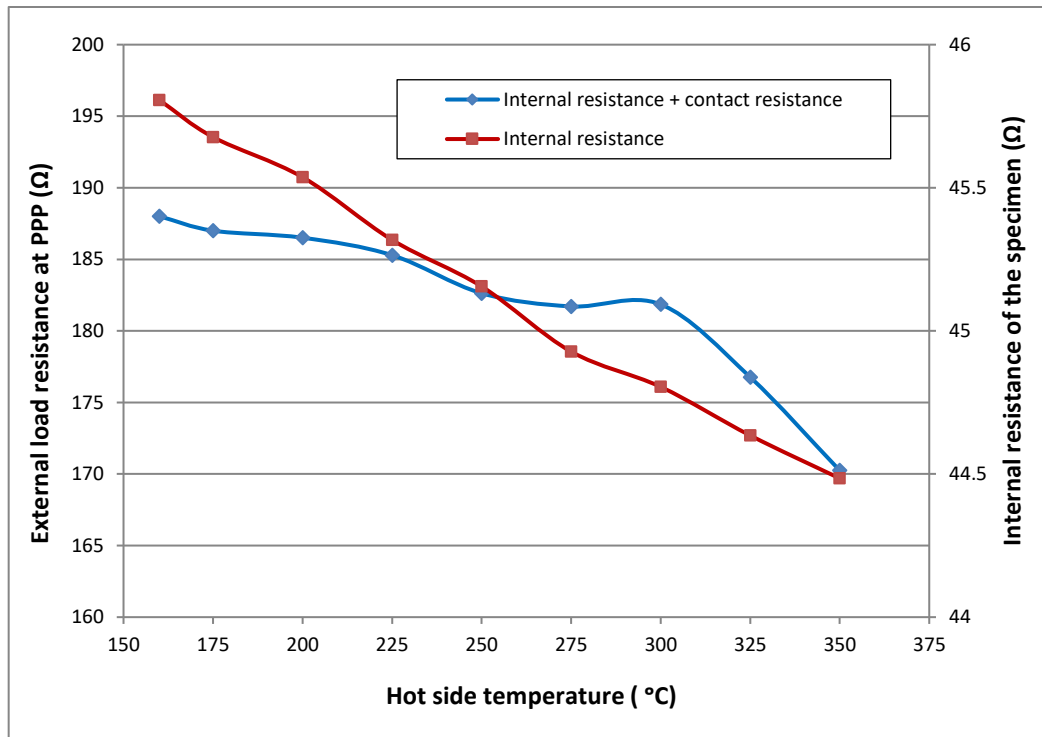


Fig. 12: Electrical resistance with /without considering contact resistance

413

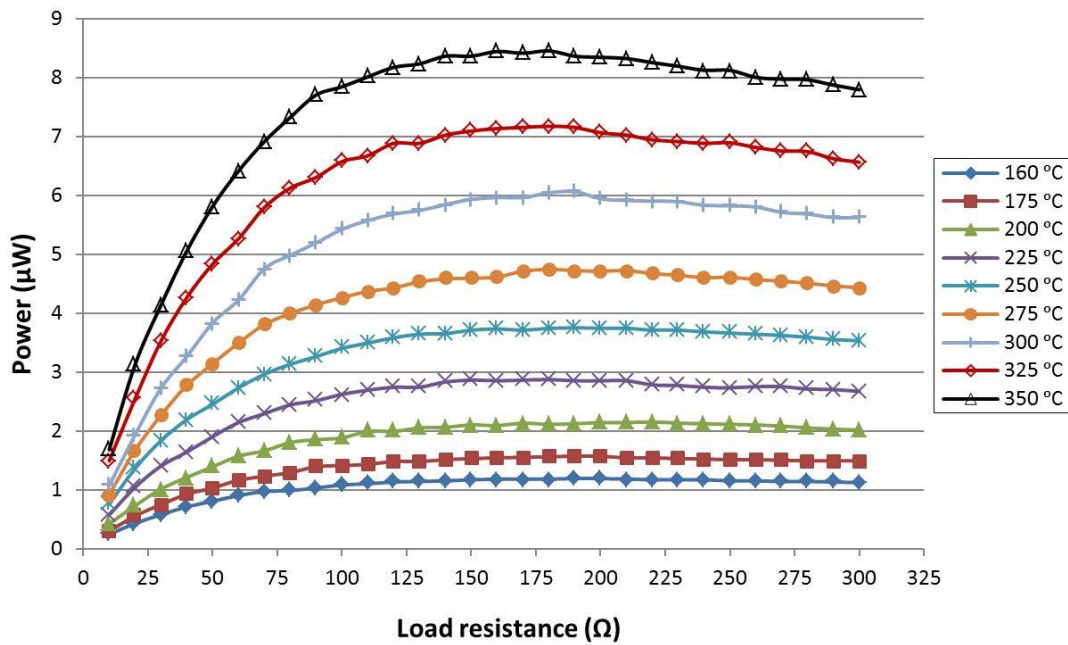


Fig.13: Output power by considering contact resistance versus applied load resistances

414

415

416

417

418

419

420

421

422

423

424

425

426

427

428

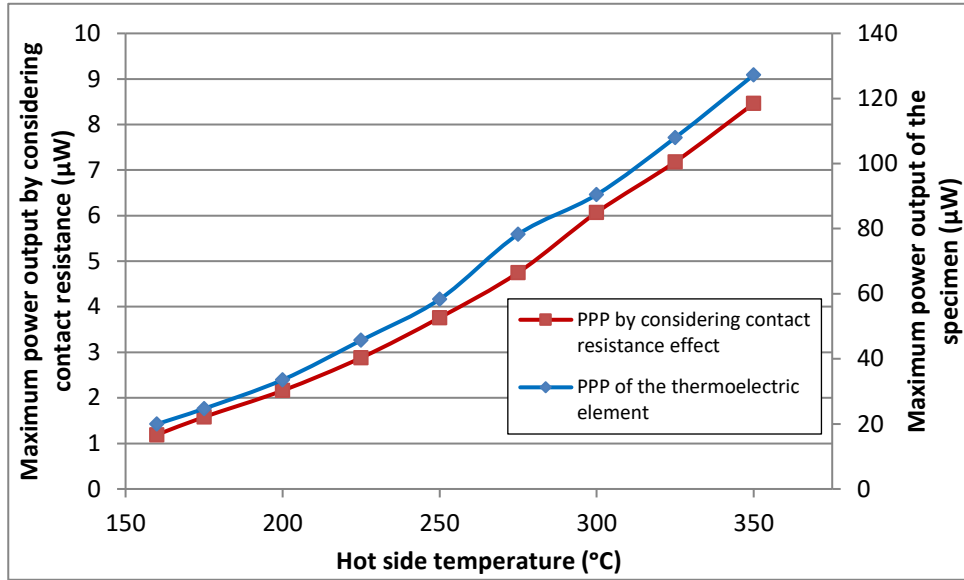


Fig. 14: Maximum power output with/without considering contact resistance effect

430

431

### 432 Tables

433

434

435

Table 1: Composition of the film determined by EDX

at% (Zn)	$\sigma$ (at% (Zn))	at% (Sb)	$\sigma$ (at% (Sb))
57.6	1.8	42.4	1.3

436